How much of Typhoon Morakot's extreme rainfall is attributable to anthropogenic climate change?

Chung-Chieh Wang[1], Li-Shan Tseng[1]*, Chien-Chang Huang[2], Shih-How Lo[1], Cheng-Ta Chen[1], Pi-Yu Chuang[1], Nan-Chou Su[1], and K. Tsuboki[3]

[1]Department of Earth Sciences, National Taiwan Normal University, Taipei, Taiwan.

[2]Department of Atmospheric Sciences, National Taiwan University, Taipei, Taiwan.

[3]Institute for Space-Earth Environmental Research, Nagoya University, Nagoya, Japan.

*Corresponding author: **Li-Shan Tseng**
Address: B406 Science Building, No. 88 Sec. 4 Ting-Chou Road, Wen-Shan District, Taipei 11677, Taiwan (R. O. C.)
E-mail: sian@ntnu.edu.tw
Phone: 886-2-7734-6410
Fax: 886-2-2933-3315

Short Title: Extreme rainfall of Typhoon Morakot (2009) and climate change

Key Words:

- Extreme rainfall
- Anthropogenic climate change
- Sensitivity experiments
- Water budget analysis
- Secondary circulation

Abstract

Typhoon Morakot (2009), which made landfall in Taiwan during 7–9 August 2009, produced the highest rainfall and became the deadliest typhoon ever recorded in Taiwan since 1958. To assess the role of anthropogenic climate change in the typhoon-related torrent, we compare the water budget between a pair of cloud-resolving sensitivity experiments. The pair consists of a control simulation that reproduces Typhoon Morakot (2009) in current climate and a sensitivity simulation in which the same storm is placed in a slightly different climate background where the late-20th-century anthropogenic climate change signal is removed. The anthropogenic signal is estimated with the CMIP 5 experiments of 18 models for the period of 1985–2005, during which the global warming trend is discernible. In climate states that differ merely by a 20-year mean anthropogenic change, Morakot (2009) yields 3.4%–3.6% more total rainfall in the control experiment than its sensitivity counterpart within a radius of 300–500 km from the storm center. Water budget analysis indicates that the increase in typhoon rainfall is mainly resulted from the enhanced convergence of vapor flux. The enhancement is, in turn, contributed by the increased tropospheric moisture due to global warming and, to a lesser extent, by a more active secondary circulation in the storm that is associated with the anthropogenic climate change.

1. Introduction

Morakot (2009) formed as tropical depression late on August 2 and soon developed into tropical storm and had its name assigned on August 3 by the Japan Meteorological Agency (JMA). It moved approximately westward toward Taiwan and gradually intensified to typhoon status late on August 5. After continuous strengthening to its peak intensity of ~40 m/s (according to JMA) on the following day, Morakot began to move slower due to the weakening high-level steering flow (down to ~16.3 km/hr right before making landfall in Taiwan around 1600 UTC 7 August, according to the Central Weather Bureau (CWB) of Taiwan). The translation speed continued to reduce to ~9.1 km/hr during landfall and went even more slowly after exiting the island at ~7.7 km/h headed northwestward (Wang et al., 2012 and 2013). Owing to its slow movement, the storm influence period on Taiwan was estimated to be as long as 64 hours (Chien and Kuo, 2011). During the warning period, Morakot produced record-breaking rainfall (e.g., 2858.5 mm at ALiShan station), wreaked havoc in southern part of the island, and became the deadliest typhoon in Taiwan since 1958.

The prolonged heavy rainfall of Morakot is generally accepted to be ascribable to a strong southwest summer monsoon flow that interacts with the steep topography of Taiwan (Chien and Kuo, 2011; Wang et al., 2012; Huang et al., 2014). Figure 1 shows the large-scale circulation backdrop prior to the development of Morakot. A southeastward protruding monsoon trough, a feature of the second phase of East Asian summer monsoon (Hsu, 2005), extended as far as 150°E. Hong et al., (2010) found 30–60-day and 10–30-day intraseasonal oscillations present during that period, with the latter actively growing since

July. Low-level circulation of the strengthened monsoon trough became organized as a circular vortex nearly 2500 km wide extending eastward from SCS, Luzon island, and into the Philippine Sea/western North Pacific Ocean (Figure 1), with a band of deep convective clouds rimming the southern-through-eastern periphery of the vortex (not shown). This was the monsoon gyre (Lander, 1994) that spawned Typhoons Goni, Morakot, and Etau in succession, among which Goni was thought to be important at a later stage in conveying moisture supply to Morakot from as far as Bay of Bengal (Chien and Kuo, 2011; Lee et al., 2011). The moisture-laden monsoonal flows interacted with the typhoon circulation to form a series of deep mesoscale convective systems over southern Taiwan Strait and to steer them onshore into Taiwan. Asymmetric latent heat release around the typhoon might add to the synoptic-scale effect of weak steering flow on slowing down the translation speed of Morakot via a convective-scale nonlinear dynamical process (Wang et al., 2015a), especially during the exit phase off the island (Wang et al., 2012; Hsu et al., 2013; Chen et al., 2016). It was the synergy among all these favorable factors across different scales why Lee et al. (2011) dubbed Morakot (2009) the “perfect monsoon-influenced typhoon” and that led to the record rainfall accumulation and subsequent disaster (Wang et al., 2012).

Aside from the concurrence and interaction among storm-scale convection, synoptic-scale typhoon circulation, intraseasonal disturbances, and seasonal monsoon flow, the torrential rain of Morakot (2009) may also owe, at least, partly to the long-term climate change. Chang et al. (2013) shows that Taiwan experiences a dramatic increase in typhoon-related rainfall in the beginning of the 21st century, with seven out of the top ten rain-producing typhoons occurring after year 2000, of which Morakot ranks the first. Current

theoretical and modeling studies of global greenhouse warming mostly project an increase in tropical cyclone (TC) intensity along with storm-related precipitation rate (Knutson et al., 2010). For the case of Morakot, however, the catastrophic torrent of rainfall is accompanied by a maximum wind speed of barely 80 Knots (category 1). TC activities in the western North Pacific (WNP) have been found to vary with SSTs on interannual and decadal scales (Chan, 2008; Knutson et al., 2010; Lau and Zhou, 2012), whereas the trend on scales of half a century or more is somewhat mixed among different TC paths (Chang et al., 2012). Attribution between forcing of anthropogenic and natural sources is complicated with observational data. In current study, we will focus on the influence of the anthropogenic forcing on TC rainfall. With the help of a high-resolution cloud-resolving model, we can quantitatively assess the effect of the model-estimated late 20^{th} century anthropogenic climate change on the top rain-producing typhoon Morakot (2009).

This article first describes the model, data, and experiment design in section 2. Section 3 presents the main results from the simulations, followed by discussion and concluding remarks in sections 4 and 5.

2. Methodology and Experiments

We employ the Cloud-Resolving Storm Simulator (CReSS) of Nagoya University, Japan (Tsuboki and Sakakibara, 2002 and 2007) for the high-resolution numerical experiments at a grid size of 3 km and 40 vertical levels in a 2400 km × 1800 km domain, with physical options similar to those used in Wang et al. (2015b). The lower boundary conditions are a 1 km × 1 km real topography and the $1^{\circ} \times 1^{\circ}$ NOAA Optimum Interpolation (OI) SST V2 data (Reynolds et al., 2002). The initial and lateral boundary

conditions are the European Center for Medium-range Weather Forecasts (ECMWF, or EC for simplicity) $0.25^\circ \times 0.25^\circ$ 6-hourly Year of Tropical Convection (YOTC) analysis (Waliser and Moncrieff, 2007). Typhoon Morakot (2009) is reproduced in a control experiment (CE) running for 8 days during 3–10 August 2009.

A sensitivity experiment (SE_a) is carried out with all model configurations kept identical as in CE, except for the long-term anthropogenic climate change being subtracted from the initial/boundary condition for major variables including temperature, humidity, winds at surface and all pressure levels, and SST, etc (with topography excluded). The estimate of anthropogenic climate change, denoted as $\boldsymbol{\Delta}_{\text{anthrop}}$, is derived from the Coupled Model Intercomparison Project Phase 5 (CMIP5) (Taylor et al., 2009) experiments, by taking difference between the 20th century historical run and its natural counterpart and averaging it through time and among 18 models:

$$\Delta_{\text{anthrop}} = \text{ensemble mean}(\text{historical run} - \text{natural run})_{1985\text{–}2005}$$

where "ensemble mean" consists of 18 CMIP5 models as listed in Table 1, and 1985–2005 signifies the year range for time average. Through the time average, variations of time scale up to decadal range may be removed. Through the model ensemble mean, bias of individual models is largely lessened, and the influence of internal decadal variability can be reduced further. We choose years 1985–2005 because: (1) Prior to 1985, the anthropogenic signal (*i.e.* historical run – natural run) is small and generally within the range of the ensemble spread; (2) Only a handful of post-2005 model output is available in the CMIP5 archive. The period of 1985–2005 provides the largest number for ensemble members.

Main features of the model-estimated long-term anthropogenic climate change signal near Taiwan include:

(i) A small low-level cyclonic flow trend in the climatological location of westward extending subtropical high (Figure 2a), indicating an anthropogenically-forced eastward retreat of the present-day subtropical ridge.

(ii) Slightly stronger mid-level westerlies (by about 0.2–0.6 m s^{-1}) (Figure 2b) in most areas to the south of 25°N. This, along with the eastward retreat of low-level subtropical ridge, implies a weaker steering flow for westward and northwestward moving TCs that are heading to Taiwan.

(iii) Warmer (~0.5 K over ocean and higher over land) and moister lower troposphere (Figure 2c). Both fields have their maxima lying over the subtropical WNP where Morokot (2009) initiated and developed. The overall 0.4–0.6 g/kg increase of specific humidity inside the model domain is equivalent to about 4–5% moisture increase.

(iv) An SST increase more than 0.4 K to the south of 25°N (Figure 2d).

It is worth mentioning that Morakot develops around the onset of the WNP summer monsoon, during which the subtropical ridge shifts northward from approximately 25°N to 35°N and the monsoon trough and WNP convection belts are strengthening towards their mature stage into August (Zhou et al., 2011). With such a seasonal background, subtracting the above anthropogenic climate change signal from current climate state will create an environment in which there is slightly more westward-extruding subtropical ridge, weaker monsoon trough, stronger mid-level steering flow, cooler and drier atmosphere, and cooler

ocean surface (Figure S1). In the sensitivity experiment (SE_a), Typhoon Morakot is placed in such anthropogenic-forcing-free environment but driven by the same synoptic forcing as in CE.

The differences between the simulations of CE–SE_a pair can be viewed as the effects of long-term anthropogenic climate change, provided that the two modeled typhoons evolve in a similar fashion and do not bifurcate in simulations.

In the following section, we will present the simulation results of CE and SE_a. We then examine their water budget and quantify in percentages the attribution of typhoon-related precipitation in order to understand the underlying physical processes.

3. Simulation Results

The simulated track of Morakot (2009) in CE compares well with the JMA best track except for the first two days, August 3–4, when Morakot is just named and has not been upgraded to typhoon level by either JMA or JTWC (Figure 3a). The temporal evolution of typhoon intensity shows close agreement with the observation in terms of minimum sea level pressure and maximum surface wind speed, though the pressure values are somewhat lower than the JMA estimates by 5–10 hPa most of the time (Figure 3b). This degree of difference between simulated intensity and observationally-based estimates is not uncommon in previous studies using different high-resolution models (e.g. Huang et al., 2014). We examined two other best track data by JTWC and CWB and found that, for minimum sea level pressure, the estimated values often differ from one dataset to another, and the difference is generally also in the range of 5–10 hPa.

The simulated peak intensity, no matter its minimum pressure, maximum wind speed, or its time of occurrence, compares well with the observation (Figure 3, b and c). However, the post-peak weakening is not as sharp as that shown in the JMA estimates. This discrepancy may be mainly associated with the steep terrain of Taiwan and the lack of oceanic feedback in our model setting. For the concern of terrain, the steep Central Mountain Range acts to weaken the storm intensity and may not be sufficiently represented in the model even with the 3 km resolution due to the acute elevation gain of 4000 m in a distance as short as 50 km. For the role of ocean, Zheng et al. (2014) used a regional ocean model along with the Argo data to show that, in response to the passage of Morakot, an offshore cool jet originating from the southeastern tip of Taiwan was generated and extended northward along the Kuroshio, resulting in a quick and drastic SST drop. This TC-induced cooling may significantly reduce the strength of the TC itself, especially for a slow-moving typhoon such as Morakot (Schade and Emanuel, 1999; Lin et al., 2009). In our atmosphere-only model, the oceanic negative feedback is absent and therefore the simulated typhoon intensity tends to be higher than the observed.

In the anthropogenic sensitivity experiment (SE_a), the simulated temporal evolution is similar to that in CE. The track also exhibits only small differences from that in CE (Figure 3a). These similarities are expected since climate backdrops of the two experiments are not far from each other. Nevertheless, a discernible westward shift, albeit small, appears in the simulated trajectory in SE_a right before the typhoon makes landfall in Taiwan. This tendency remains throughout later stages of its life cycle, presumably a direct result of its slightly faster translation speed driven by a slightly stronger steering flow in a climate state

free of anthropogenic forcing. The more obvious trajectory shift after, compared to before, landfall is probably because of reduced nonlinear interactions among typhoon circulation, mesoscale convective systems, and topography under the influence of cooler and less-moisture-laden monsoonal flows (Wang et al., 2012; Hsu et al., 2013; Wang et al., 2015a; Chen et al., 2016). This leads to slightly shorter landfall duration over Taiwan in SE_a.

Figure 4 shows satellite observation from the Tropical Rainfall Measurement Mission (TRMM) or Aqua-1 at selected times that have better coverage of Morakot (2009) (Figure 4, middle column). We compare them at closest model output times with rainfall distribution of the CE/SE simulation driven by the EC YOTC analysis data (Figure 4, left/right column). It is shown that the CReSS model realistically reproduces many aspects of the typhoon rainfall structure, including the weak inner core and large asymmetric outer rain bands. The total accumulated rainfall during the warning period (6–10 August) also matches the CWB rain gauge measurements (Figure 5). However, snapshots of the CE–SE_a difference display opposite signs in a random fashion both in space and time. For our purpose to examine typhoon-related rainfall changes in different climate states, it is easier to compare by averaging rainfall amount both in space and time.

The simulated areal-mean typhoon rainfall of both experiments is summarized in Table 2. It shows an overall higher rainfall amount in CE, as is expected in the slightly moister and warmer environment of current climate. The increase of total rainfall throughout the simulation period ranges between 2.5% and 3.6%, depending on the radius considered for the calculation of areal mean values (Table 2, left half). The largest increase takes place at the range of 300 km, of which the daily allocation is shown in the right half

of Table 2. The heaviest rainfall occurs during August 6–8 in both experiments, in agreement with the observation, and the CE–SE$_a$ difference shows consistent increase for each individual days. These results align with those of Donat et al. (2016), who found increases in annual-maximum daily precipitation (Rx1day) in Southeast Asia during 1951–2010. To confirm the robustness of the overall increase in simulated typhoon-related rainfall under climate change, we perform the one-tail *t* test for paired samples (Barber, 2009). Here we test whether the CE–SE$_a$ differences of areal mean daily rainfall within 300 km from the storm center are significant over the simulation period of 3–10 August. At confidence level of 0.975, the *t* test rejects the null hypothesis that mean daily rainfall of Typhoon Morakot does not increase. The result suggests that the overall simulated rainfall increase of Typhoon Morakot brought about by the anthropogenic climate change is statistically significant and does not arise from random processes in the model.

Water budget analysis

In order to understand the source of the increased rainfall associated with typhoon Morakot (2009), a water budget analysis is carried out for a cylindrical column around the storm center with varying radius. We adopt the budget equation of *Trenberth and Guillemot* (1995), partitioning the water substance into vapor and suspending condensates (*i.e.*, hydrometeors), and rewrite the equation as

$$P + \frac{\partial}{\partial t}(w_v + w_h) = -\int_0^\infty \nabla \cdot (\rho_v \mathbf{V}) dz - \int_0^\infty \nabla \cdot (\rho_h \mathbf{V}) dz + E + R, \quad (1)$$

TDC *CVF* *CHF*

where P is precipitation, w_v and w_h are the vapor and hydrometeor contents in the column, ρ_v and ρ_h are vapor and hydrometeor density, $\mathbf{V}$ is horizontal wind, E is evaporation, and R is residual term. The total water content, $w_v + w_h$, in the tendency (*TDC*) term is defined as

$$w_v + w_h = \int_0^\infty (\rho_v + \rho_h) dz. \tag{2}$$

For a fixed volume of air column, Eq. (1) states that convergence of vapor flux (*CVF*), convergence of hydrometeor flux (*CHF*), and evaporation are the source of water that either falls out as precipitation (*P*) or stays to moisten the air (*TDC*). The *CVF* term can be divided as

$$\underbrace{-\int_0^\infty \boldsymbol{\nabla} \cdot (\rho_v \mathbf{V}) dz}_{CVF} = \underbrace{-\int_0^\infty \rho_v (\boldsymbol{\nabla} \cdot \mathbf{V}) dz}_{CONV} \underbrace{- \int_0^\infty (\mathbf{V} \cdot \boldsymbol{\nabla}) \rho_v dz}_{ADV}, \tag{3}$$

which decomposes the convergence of vapor flux (*CVF*) into convergence (*CONV*) and advection (*ADV*) components.

The above water budget calculation is performed for a cylindrical column with different radii around the storm center. The results averaged within 400 km of radius and over the period of heaviest rainfall during 5–10 August are summarized in Table 3. In both experiments, the mean rainfall (*P*) mainly comes from the *CVF* (86%–87%) across the lateral boundaries. The second largest term is local evaporation (*E*) from the underlying ocean, which is an order of magnitude smaller than *CVF* and contributes about 10% to *P*. The remaining *TDC*, *CHF*, and *R* terms are all small and each contributes only 0.5%–2.1% to *P*. The *CVF* is predominantly attributed to the *CONV* term, while *ADV* has a small

257 negative contribution due to the typical low-level dry inflow of typhoons from their
258 surroundings.

259 For the differences between CE and SE_a, the excessive mean rainfall of present-day
260 Morakot (CE−SE_a) is again mainly from the enhanced *CVF*, which contributes 11 times
261 more than the second largest term of enhanced *E*. The enhanced *CVF* is yet again due to the
262 predominant increase in *CONV* over the also enhanced negative effect of *ADV*.
263 Contributions to the *CONV* component can further be roughly estimated as those from the
264 lower tropospheric precipitable water ($PW_{5.5}$) and vertically integrated horizontal
265 convergence ($IHC_{5.5}$):

266 $$PW_{5.5} = \int_0^{5.5\ \mathrm{km}} \rho_v dz, \text{ and} \quad (4)$$

267 $$IHC_{5.5} = -\int_0^{5.5\ \mathrm{km}} (\boldsymbol{\nabla} \cdot \mathbf{V}) dz. \quad (5)$$

268 The former describes the tropospheric thermodynamic state that is controlled by the large-
269 scale environment, and the latter signifies the activeness of the typhoon secondary
270 circulation. The decomposition of *CONV* in Table 3 shows that its increase owes
271 predominantly to the change in tropospheric moisture content and, to a lesser extent, to the
272 adjustment in storm secondary circulation (3.6% vs. 1.1%). It is worth noted that the 3.6%
273 increase in $PW_{5.5}$ responding to the anthropogenically forced 0.4–0.5 K warming of SST
274 along the typhoon track (Figure 2d) amounts to an increase rate at 7.2%–9% per degree,
275 which roughly conforms to the Clausius-Clapeyron rate of 7% per degree.

4. Discussion

The water budget analysis for the simulated Typhoon Morakot (2009) demonstrates that, under the anthropogenic warming trend in global climate, storm rainfall increases roughly in line with water vapor increase and enhanced dynamical convergence. However, percentage increase of rainfall (*P*: 2.2%) is less than that of vapor flux convergence (*CVF*: 3.9%). Although the difference is not huge, we notice that the discrepancy is mainly due to the residual term, *R*, whose value rises more than three times from 0.017 mm h^{-1} in CE to 0.073 mm h^{-1} in SE_a. In the calculation of water budget for each model output interval of 3 hours, we use accumulated amount for precipitation and instantaneous values for all other variables; this choice could, at least partially, contribute to the drastic rise in *R*. Intuitively, reducing the model output interval may help lower the fluctuation. We tried the interval of 1 hour in some similar experiment sets for other typhoon cases but still found sizeable fluctuations in *R* from one experiment to another. Despite the described fluctuations, *R* is always much smaller (by more than an order of magnitude) than the two leading terms of *P* and *CVF*, and conclusions based on the water budget equations (1)~(5) should not be affected. Another issue that may account for the discrepancy between *P* and *CVF* is to do with the flow field used in the water budget calculation. In contrast to the vortex-relative wind used in some previous studies (e.g., Yang et al., 2001), here we use ground-relative wind without taking into account the slow translation speed of Morakot (2009). In view of the smallness of both *CHF* and *R*, and considering that switching the wind from ground-relative to vortex-relative will change only *CVF*, *ADV*, *CHF*, and *R*, we can expect *CVF*

297 remains to be the dominant contributor to *P* and our conclusions based on water budget
298 analysis stay unchanged.

299 Figure 6 shows the mean temperature profiles averaged over the model domain and
300 the simulated period of 3–8 August for both experiments, together with the profile of their
301 difference. As is expected from the IPCC AR5 (2013) and previous observational and
302 modeling studies (e.g. Pawson and Fiorino, 1998; Santer et al., 2004; Vecchi et al., 2013),
303 we see stratospheric cooling accompanied by tropospheric warming, with the warming
304 amplitude at upper troposphere roughly 1.8 times that of the surface. In the slightly stabler
305 troposphere in CE than SE_a, central pressure of Morakot (2009) appears somewhat
306 deepened even though the maximum wind speed does not change much (Figure 3).
307 Moreover, the storm precipitation and associated water transport are enhanced despite of
308 the upper tropospheric stabilization (Tables 2 and 3). These signals seem to be in agreement
309 with the late-21st-century climate change studies of Tuleya et al. (2016) and Knutson et al.
310 (2013 and 2015) where they demonstrate that upper-tropospheric warming does not
311 completely negate the surface warming effect. The water budget of our experiments shows
312 that the anthropogenically forced surface warming acts to increase precipitable water in the
313 air and to enhance the storm's secondary circulation. Although the strengthened secondary
314 circulation tends to bring more dry air into the storm, it converges in even more water
315 vapor to counteract the drying effect and contribute to the precipitation increase of
316 Typhoon Morakot (2009).

317 A caveat is worth making here: There are many factors known to affect the
318 formation and development of tropical cyclones, such as SSTs, temperature, moisture, and

large-scale circulation in storm environment that are considered in this study. But many questions remain about how weak incipient disturbance (such as thunderstorm clusters) go on to evolve into a typhoon, and we are not sure how anthropogenic forcing affected the likelihood of occurrence for storm events like Morakot. Our attribution conclusion is an ingredients-based assessment where the aforementioned ingredients (SSTs, etc.) for the event were changed by anthropogenic warming. In such an experiment setting, enhanced typhoon-related rainfall and its secondary circulation attributable to anthropogenic climate change, but nothing can be said about the frequency of occurrence for such events.

5. Concluding Remarks

To quantitatively assess how much rainfall of Typhoon Morakot (2009) could have been enhanced by historical anthropogenic forcing, we perform a cloud-resolving simulation of the storm and test its sensitivity by placing it in a climate background that has the anthropogenic forcing removed. The anthropogenic forcing is estimated using CMIP5 Experiments by taking difference between the 20th century historical and natural runs, and then taking time average through 1985–2005 and ensemble average among 18 models in Table 1. As shown in Figures 2 and S1, the estimated anthropogenic signal in major variables exhibits a low-level cyclonic circulation trend over the Philippine Sea, a mid-level westerly trend to the south of 25°N along the southern flank of the subtropical high, a warming and moistening trend in the lower troposphere, and SST warming trend. With this anthropogenic climate change being removed in the sensitivity experiment, Typhoon Morakot is placed in a large-scale background of stronger and more westward protruding subtropical ridge, stronger mid-level steering flow for westward-moving typhoon, cooler

and drier lower troposphere, and cooler ocean surface. Although these changes are small, the approach of climate model sensitivity experiments still allows for an initial quantitative assessment of the long-term climate impacts on typhoon-related rainfall and the result is supported by one-tail *t* significant test.

Difference between the two experiments, CE–SE_a, indicates that the anthropogenic climate change works to enhance Morakot's overall rainfall by 2.5%–3.6% (Table 1). Rainfall of individual days during the simulation period also shows consistent increase by 0.4%–6.5%, with the maximum increase happens on the day of the flood—August 8. These results generally agree with Wang et al. (2015b) that simulates two other typhoons hitting Taiwan, and also Scoccimarro et al. (2014) and Villarini et al. (2014) that consider composite tropical cyclones in their climate models, as well as the observational and modeling study of Donat et al. (2016) for the 1950–2010 period. Water budget analysis in Table 2 reveals sources of the Morakot (2009) rainfall enhancement and shows that, under the influence of anthropogenically-forced warming trend, moisture increases in the lower troposphere by 3.6% and the typhoon secondary circulation becomes slightly more active by 1.1%. Consequently, the positive effect of moisture convergence and the negative effect of dry advective inflow into the typhoon are both enhanced. Results in Table 2 indicate that the former effect predominates and results in the increased convergence of water vapor flux (by 3.9%) associated with typhoon Morakot (2009).

It is worth noting that the two climate states considered here in our paired experiments are not dramatically different from each other in terms of circulation, but the control (*i.e.* present-day) experiment has a warmer and moister environment. In response to

this environmental difference, the simulated TC-related rainfall increase of 2.5%–3.6% should not be deemed trivial, considering that the warming trend is expected to continue in the foreseeable decades to come.

Acknowledgments and Data

We appreciate the anonymous reviewers for their invaluable comments and suggestions. U.S. Naval Research Laboratory (http://www.nrlmry.navy.mil/sat_products.html) is acknowledged for providing satellite products in Figure 4. We acknowledge the World Climate Research Programme's Working Group on Coupled Modelling, which is responsible for CMIP, and we thank the climate modeling groups (listed in Table 1 of this paper) for producing and making available their model output. For CMIP the U.S. Department of Energy's Program for Climate Model Diagnosis and Intercomparison provides coordinating support and led development of software infrastructure in partnership with the Global Organization for Earth System Science Portals. This study is jointly supported by the Ministry of Science and Technology of Taiwan under Grants MOST-105-2111-M-003-003-MY3, MOST-107-2625-M-003-001 and MOST-107-2635-M-003-001.

References

Burt JE, Barber GM, Rigby DL. 2009. *Elementary Statistics for Geographers*. Guilford Press, New York, USA.

Chan JCL. 2008. Decadal variation of intense typhoon occurrence in the western North Pacific. *Proc. R. Soc. A* **464**: 249–272. https://doi.org/10.1098/rspa.2007.0183

Chang CP, Lei Y, Sui CH, Lin X, Ren F. 2012. Tropical cyclone and extreme rainfall trends in East Asian summer monsoon since mid-20th century. *Geophys. Res. Lett.* **39**: L18702. https://doi.org/10.1029/2012GL052945

Chang CP, Yang YT, Kuo HC. 2013. Large increasing trend of tropical cyclone rainfall in Taiwan and the roles of terrain. *J. Climate* **26**: 4138–4147. https://doi.org/10.1175/JCLI-D-12-00463.1

Chen YH, Kuo HC, Wang CC, Yang YT. 2017. Influence of southwest monsoon flow and typhoon motion on Taiwan rainfall during the exit phase. *Q. J. Roy. Meteor. Soc.* **143**: 3014–3024. https://doi.org/10.1002/qj.3156

Chien FC, Kuo HC. 2011. On the extreme rainfall of Typhoon Morakot (2009). *J. Geophys. Res.* **116**: D05104. https://doi.org/10.1029/2010JD015092

Donat MG, Lowry AL, Alexander LV, O'Gorman PA., Maher N. 2016. More extreme precipitation in the world's dry and wet regions. *Nature Climate Change* **6**: 508–513. https://doi.org/10.1038/nclimate2941

Hong CC, Lee MY, Hsu HH, Kuo JL. 2010. Role of submonthly disturbance and 40-50 day ISO on the extreme rainfall event associated with Typhoon Morakot (2009) in southern Taiwan. *Geophys. Res. Lett.* **37**: L08805. https://doi.org/10.1029/2010GL042761

Hsu HH. 2005. Intraseasonal variability of the atmosphere-ocean-climate system: East Asian monsoon. *Intraseasonal Variability in the Atmosphere-Ocean Climate System*. Springer-Verlag Berlin Heidelberg: New York, USA.

Hsu LH, Kuo HC, Fovell RG. 2013. On the geographic asymmetry of typhoon translation speed across the mountainous island of Taiwan. *J. Atmos. Sci.* **70**: 1006–1022.

405 Huang HL, Yang MJ, Sui CH. 2014. Water budget and precipitation efficiency of Typhoon
406 Morakot (2009). *J. Atmos. Sci.* **71**: 112–129.
407 IPCC (2013) *The Physical Science Basis. Contribution of Working Group I to the Fifth*
408 *Assessment Report of the Intergovernmental Panel on Climate Change* (Eds. Stocker TF,
409 Qin D, Plattner GK, Tignor M, Allen SK, Boschung J, Nauels A, Xia Y, Bex V,
410 Midgley PM). Cambridge University Press.
411 Kalnay E, et al. 1996. The NCEP/NCAR 40-Year Reanalysis Project. *Bull. Amer. Meteor.*
412 *Soc.* **77**: 437–471.
413 Knutson TR, et al. 2010. Tropical cyclones and climate change. *Nat. Geosci.* **3**: 157–163.
414 https://doi.org/10.1038/ngeo779
415 Knutson TR, et al. 2013. Dynamical downscaling projections of twenty-first-century
416 Atlantic hurricane activity: CMIP3 and CMIP5 model-based scenarios. *J. Clim.* **26**:
417 6591–6617. https://doi.org/10.1175/JCLI-D-12-00539.1
418 Knutson TR, et al. 2015. Global projections of intense tropical cyclone activity for the late
419 twenty-first century from dynamical downscaling of CMIP5/RCP4.5 Scenarios. *J. Clim.*
420 **28**: 7203–7224. https://doi.org/10.1175/JCLI-D-15-0129.1
421 Lander MA. 1994. Description of a monsoon gyre and its effects on the tropical cyclones in
422 the western North Pacific during August 1991. *Wea. Forecasting*. **9**: 640–654.
423 Lau WKM, Zhou YP. 2012. Observed recent trends in tropical cyclone rainfall over the
424 North Atlantic and the North Pacific. *J. Geophys. Res.* **117**: D03104.
425 https://doi.org/10.1029/2011JD016510
426 Lee CS, Wu CC, Chen Wang TC, Elsberry RL. 2011. Advances in understanding the
427 “perfect monsoon-influenced typhoon”: Summary from International Conference on

428 Typhoon Morakot (2009). *Asia-Pacific J. Atmos. Sci.* **47**: 213-222.
429 https://doi.org/10.1007/s13143-011-0010-2
430 Lin II, Pun IF, Wu CC. 2009. Upper ocean thermal structure and the western North Pacific
431 category-5 typhoons. Part II: Dependence on translation speed. *Mon. Wea. Rev.* **137**:
432 3744–3757. https://doi.org/10.1175/2009MWR2713.1
433 Pawson S, Fiorino M. 1998. A comparison of reanalyses in the tropical stratosphere. Part 1:
434 Thermal structure and the annual cycle. *Climate Dyn.* **14**: 631–644.
435 Rayner NA, Parker DE, Horton EB, Folland CK, Alexander LV, Rowell DP, Kent EC,
436 Kaplan A. 2003. Global analyses of sea surface temperature, sea ice, and night marine
437 air temperature since the late nineteenth century. *J. Geophys. Res.* **108**: 4407–4444.
438 https://doi.org/10.1029/2002JD002670
439 Reynolds RW, Rayner NA, Smith TM, Stokes DC, Wang W. 2002. An improved in situ
440 and satellite SST analysis for climate. *J. Climate* **15**: 1609–1625.
441 Santer BD. et al. 2004. Identification of anthropogenic climate change using a second-
442 generation analysis. *J. Geophys. Res.* **109**: D21104.
443 https://doi.org/10.1029/2004JD005075
444 Schade LR, Emanuel KA. 1999. The ocean's effect on the intensity of tropical cyclones:
445 Results from a simple coupled atmosphere ocean model. *J. Atmos. Sci.* **56**: 642–651.
446 Scoccimarro E, Gualdi S, Villarini G, Vecchi G, Zhao M, Walsh K, Navarra A. 2014.
447 Intense precipitation events associated with landfalling tropical cyclones in response to a
448 warmer climate and increased CO2. *J. Climate* **27**: 4642–4654.
449 https://doi.org/10.1175/JCLI-D-14-00065.1

Taylor KE, Stouffer RJ, Meehl GA. 2012. An Overview of CMIP5 and the experiment design. *Bull. Amer. Meteor. Soc.* **93**: 485-498. https://doi.org/10.1175/BAMS-D-11-00094.1

Trenberth KE, Guillemot CJ. 1995. Evaluation of the global atmospheric moisture budget as seen from analyses. *J. Climate* **8**: 2255–2272.

Tsuboki K, Sakakibara A. 2002. Large-scale parallel computing of cloud resolving storm simulator. *High Performance Computing*. Springer-Verlag Berlin Heidelberg: New York, USA.

Tsuboki K, Sakakibara A. 2007. *Numerical Prediction of High-Impact Weather Systems*. Nagoya University: Nagoya, Japan. Available from: http://www.rain.hyarc.nagoya-u.ac.jp/~tsuboki/cress_html/src_cress/CReSS2223_users_guide_eng.pdf

Tuleya RE, et al. 2016. Impact of upper-tropospheric temperature anomalies and vertical wind shear on tropical cyclone evolution using an idealized version of the operational GFDL hurricane model. *J. Atmos. Sci.* **73**: 3803–3820. https://doi.org/10.1175/JAS-D-16-0045.1

Vecchi GA, Fueglistaler S, Held IM, Knutson TR, Zhao M. 2013. Impacts of atmospheric temperature trends on tropical cyclone activity. *J. Climate* **26**: 3877–3891.

Villarini G, Lavers DA, Scoccimarro E, Zhao M, Wehner MF, Vecchi GA, Knutson TR, Reed KA. 2014. Sensitivity of tropical cyclone rainfall to idealized global scale forcings. *J. Climate* **27**: 4622–4641. https://doi.org/10.1175/JCLI-D-13-00780.1

Waliser DE, Moncrieff M. 2007. Year of the tropical convection—Joint WCRP-THORPEX activity to address the challenge of tropical convection. *WCRC GEWEX News* **17**: 8.

Wang CC, Kuo HC, Chen YH, Huang HL, Chung CH, Tsuboki K 2012. Effects of asymmetric latent heating on typhoon movement crossing Taiwan: The case of Morakot (2009) with extreme rainfall. *J. Atmos. Sci.* **69**: 3172–3196. https://doi.org/10.1175/JAS-D-11-0346.1

Wang CC, Kuo HC, Yeh TC, Chung CH, Chen YH, Huang SY, Wang YW, Liu CH. 2013. High-resolution quantitative precipitation forecasts and simulations by the Cloud-Resolving Storm Simulator (CReSS) for Typhoon Morakot (2009). *J. Hydrol.* **506**: 26–41. https://doi.org/10.1016/j.jhydrol.2013.02.018

Wang CC, Kuo HC, Johnson RH, Lee CY, Huang SY, Chen YH. 2015a. A numerical study of convection in rainbands of Typhoon Morakot (2009) with extreme rainfall: Roles of pressure perturbations with low-level wind maxima. *Atmos. Chem. Phys.* **15**: 11097–11115. https://doi.org/10.5194/acp-15-11097–2015

Wang CC, Lin BX, Chen CT, Lo SH. 2015b. Quantifying the effects of long-term climate change on tropical cyclone rainfall using a cloud-resolving model: Examples of two landfall typhoons in Taiwan. *J. Climate* **28**: 66–85. https://doi.org/10.1175/JCLI-D-14-00044.1

Yang MJ, Braun SA, Chen DS. 2001. Water budget of Typhoon Nari (2001). *Mon. Wea. Rev.* **139**: 3809–3828. https://doi.org/10.1175/MWR-D-10-05090.1

Yu JY, Neelin JD. 1997. Analytic approximations for moist convectively adjusted regions. *J. Atmos. Sci.* **54**: 1054–1063.

Zheng ZW, Zheng Q, Lee CY, Gopalakrishnan G. 2014. Transient modulation of Kuroshio upper layer flow by directly impinging typhoon Morakot in east of Taiwan in 2009. *J. Geophys. Res.* **119**: 4462–4473. https://doi.org/10.1002/2014JC010090

Zhou T, Hsu HH, Matsumoto J. 2011. Summer monsoons in East Asia, Indochina and the western North Pacific. *The Global Monsoon System: Research and Forecast*. World Scientific Publishing: Singapore.

Tables

Table 1. 18 CMIP5 models included for the estimate of anthropogenic climate change.

Model Name	Institution
BCC-CSM1.1	Beijing Climate Center, China Meteorological Administration
BNU-ESM	College of Global Change and Earth System Science, Beijing Normal University
CanESM2	Canadian Centre for Climate Modelling and Analysis
CCSM4	University of Miami – RSMAS
CNRM-CM5	Centre National de Recherches Météorologiques / Centre Européen de Recherche et Formation Avancée en Calcul Scientifique
CSIRO-Mk3.6.0	Commonwealth Scientific and Industrial Research Organization in collaboration with Queensland Climate Change Centre of Excellence
FGOALS-g2	LASG, Institute of Atmospheric Physics, Chinese Academy of Sciences and CESS,Tsinghua University
GFDL-CM3	NOAA Geophysical Fluid Dynamics Laboratory
GFDL-ESM2M	
GISS-E2-H	NASA Goddard Institute for Space Studies
GISS-E2-R	
HadGEM2-ES	Instituto Nacional de Pesquisas Espaciais
IPSL-CM5A-LR	Institut Pierre-Simon Laplace
IPSL-CM5A-MR	
MIROC-ESM	Japan Agency for Marine-Earth Science and Technology, Atmosphere and Ocean Research Institute (The University of Tokyo), and National Institute for Environmental Studies
MIROC-ESM-CHEM	
MRI-CGCM3	Meteorological Research Institute
NorESM1-M	Norwegian Climate Centre

503 **Table 2.** Model simulated areal-mean rainfall of typhoon Morakot for control (CE) and
504 sensitivity (SE_a) experiments, their difference ($CE - SE_a$), and the corresponding
505 percentage change [$(CE - SE_a)/CE$]. Left panels are areal-mean inside radii of 200–500 km
506 from the typhoon center and averaged over the whole simulation period of 3–10 August
507 2009. Right panels are areal-mean of the 300-km radius circle for each day. Rainfall and
508 the $CE - SE_a$ difference are in units of mm day^{-1}, and the percentage change is in unit of %.

EC YOTC	Areal-mean inside different radius *r* (km) during August 3–10 (mm day^{-1})				Areal-mean inside *r* = ***300*** km for individual days (mm day^{-1})							
	200	***300***	**400**	**500**	**8/3**	**8/4**	**8/5**	**8/6**	***8/7***	***8/8***	**8/9**	**8/10**
CE	123.1	***112.2***	83.7	61.2	67.8	92.9	114.4	***158.5***	***186.5***	***166.9***	84.1	26.4
SE_a	120.0	***108.4***	80.7	59.1	67.5	92.3	113.4	***156.2***	***176.5***	***156.1***	79.0	26.1
$CE - SE_a$	3.1	***3.8***	3.0	2.1	0.3	0.6	1.0	2.3	***10.0***	***10.8***	5.1	0.3
$\frac{CE-SE_a}{CE}$ (%)	2.5	***3.4***	3.6	3.4	0.4	0.6	0.9	1.5	***5.4***	***6.5***	6.1	1.1

509
510 **Table 3.** Water budget analysis (Eq. (1)) for typhoon Morakot. Terms include precipitation
511 (*P*), tendency of total water contents (*TDC*), convergence of vapor flux (*CVF*), convergence
512 of hydrometeor flux (*CHF*), evaporation (*E*), all integrated through a cylindrical column
513 from surface to model top inside a radius of 400 km and averaged over 5–10 August. *CVF*
514 term is partitioned into convergence (*CONV*) and advection (*ADV*) component. *CONV* is
515 further compared with the precipitable water ($PW_{5.5}$) and integrated horizontal convergence
516 ($IHC_{5.5}$) below 5.5 km [see Eqs. (3)-(5) for details]. All terms are in units of kg m^{-2} h^{-1} (i.e.
517 mm h^{-1}), except for $PW_{5.5}$ (mm), $IHC_{5.5}$ (10^{-2} m s^{-1}), and their changes (%).

Experiment		*P*	*TDC*	*CVF*					*CHF*	*E*	*R*
				Total	*CONV*			*ADV*			
					Total	$PW_{5.5}$	$IHC_{5.5}$				
YOTC	CE	3.564	–0.069	3.103	3.292	62.97	5.61	–0.189	0.018	0.358	0.017
	SE_a	3.485	–0.064	2.982	3.161	60.71	5.55	–0.179	0.018	0.347	0.073
	$CE - SE_a$	0.079	–0.005	0.121	0.131	2.26	0.06	–0.010	0.000	0.011	
	$\frac{CE - SE_a}{CE}$	2.2%	7.2%	3.9%	4.0%	3.6%	1.1%	5.3%	0.0%	3.1%	

518 **Figure Caption List**

519 **Figure 1**. 850 hPa streamlines based on the EC YOTC analysis data and averaged over 27
520 July–2 August 2009, the week prior to formation of Typhoon Morakot (2009).

521 **Figure 2**. The estimated anthropogenic climate change,
522 $\Delta_{\text{anthrop}} = \text{ensemble mean}(\text{historical run} - \text{natural run})_{1985\text{–}2005}$, of geopotential
523 height (shading, in gpm) and horizontal winds (vectors, in m s^{-1}) at (a) 850 hPa and (b) 500
524 hPa, (c) temperature (contours, in K) and specific humidity (shading, in g kg^{-1}) averaged
525 over 1000–700 hPa, and (d) SST (shading, in K). Gray contours in (a) and (b) are the
526 geopotential height and in (d) the SST averaged through the simulation period of 3–10
527 August 2009. The magenta box in each panel is the domain used for the numerical model
528 simulations.

529 **Figure 3**. (a) The JMA best-track (black) and model simulated typhoon tracks (red for CE,
530 blue for SE_a) for typhoon Morakot. Figure frame coincides with the model domain. (b)
531 Time series of minimum SLP (hPa) and (c) maximum surface wind speed (m s^{-1}) from the
532 JMA best-track estimate (black) and from the simulations (red for CE, blue for SE_a).

533 **Figure 4**. TRMM PR/TMI or AQUA1 rain rate (color) overlaid on the MTSAT infrared
534 cloud imagery (at closest time) (middle panels; courtesy of Naval Research Laboratory) and
535 model simulated rain rate (color) and horizontal wind at 100 m of height (barb) for typhoon
536 Morakot in CE and SE_a (left and right panels, respectively) at selected times (a)-(d). Rain
537 rates are in units of inch h^{-1}; full barb of wind stands for 10 m s^{-1}.

538 **Figure 5**. The total accumulated rainfall during the warning period (6–10 August 2009).
539 Observation (left panel) is based on the CWB rain gauge measurements. All plots are in
540 unit of mm.
541 **Figure 6**. Mean temperature profile averaged over the model domain and the simulation
542 period 3–8 August for experiment CE (red) and SE_a (blue), together with the profile of their
543 difference (gray).

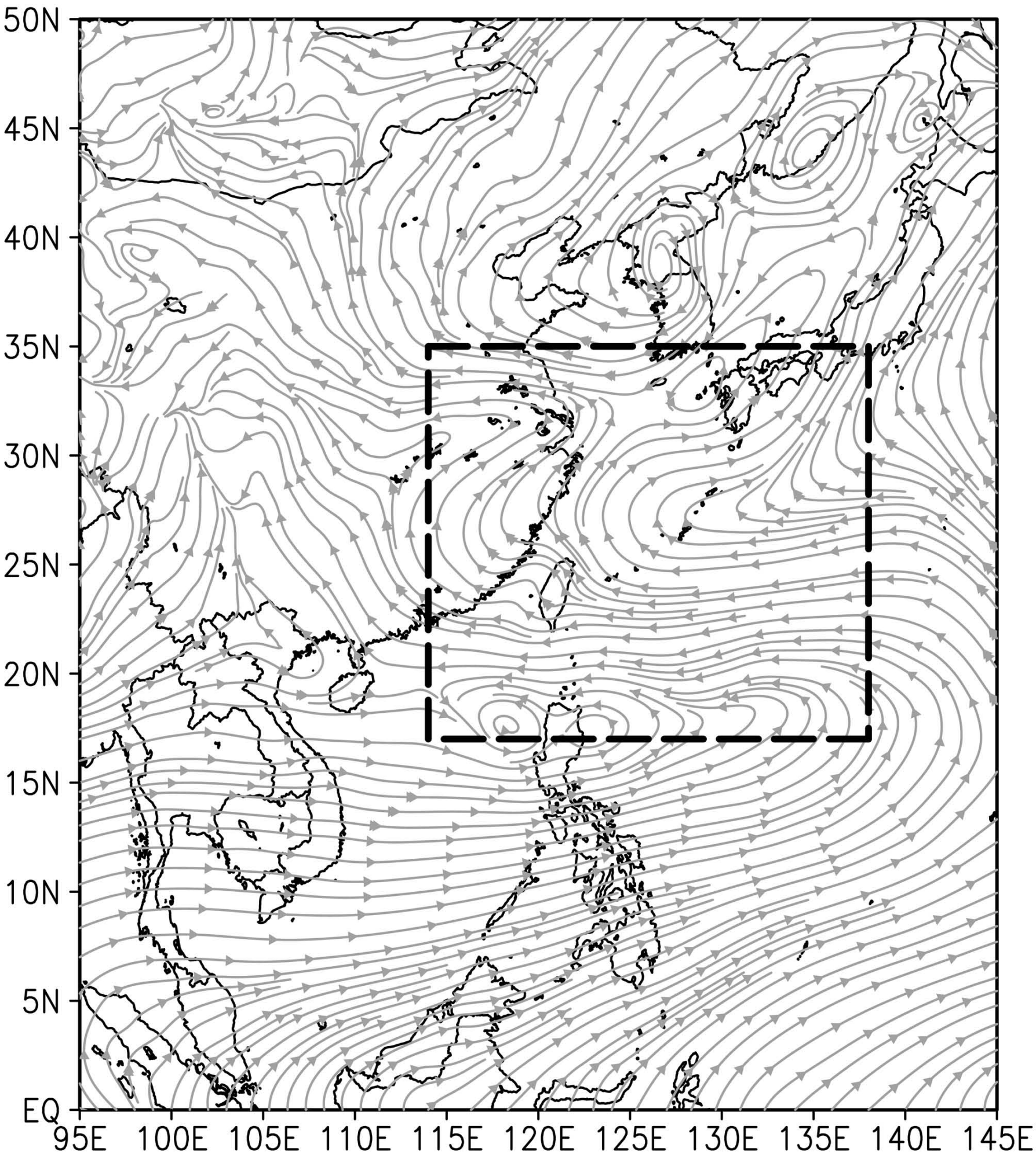
50N
45N
40N
35N
30N
25N
20N
15N
10N
5N
EQ
95E
100E
105E
110E
115E
120E
125E
130E
135E
140E
145E

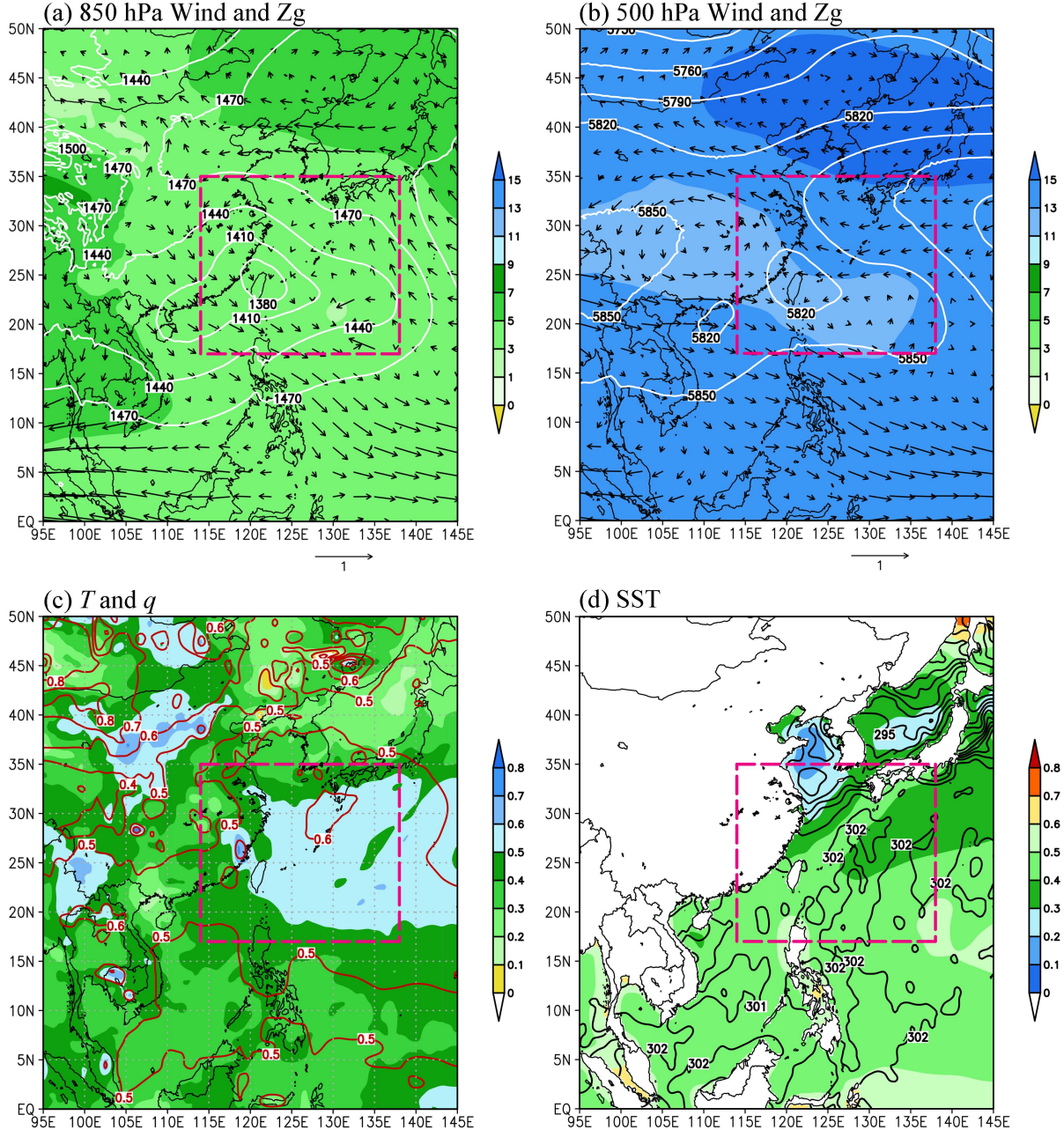
(a) 850 hPa Wind and Zg
(b) 500 hPa Wind and Zg
(c) T and q
(d) SST
50N
45N
40N
35N
30N
25N
20N
15N
10N
5N
EQ
95E 100E 105E 110E 115E 120E 125E 130E 135E 140E 145E
1
15 13 11 9 7 5 3 1 0
0.8 0.7 0.6 0.5 0.4 0.3 0.2 0.1 0

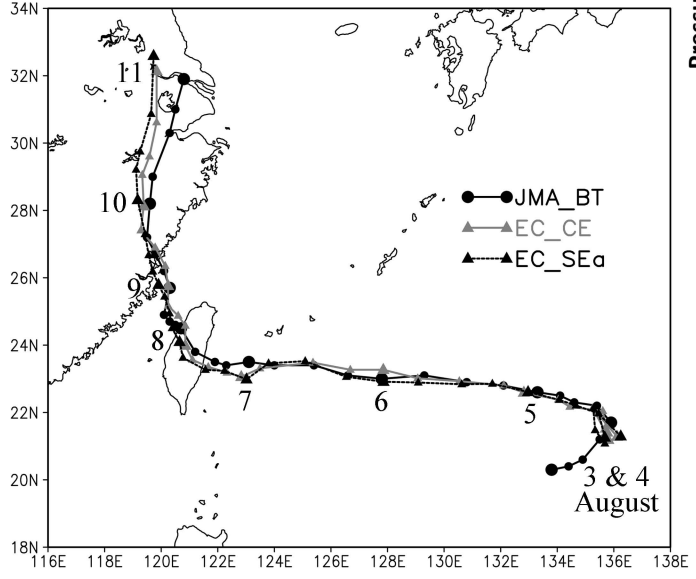
(a) TY0908 Morakot 08/03 00 Z – 08/11 00 Z
34N
32N
30N
28N
26N
24N
22N
20N
18N
116E
118E
120E
122E
124E
126E
128E
130E
132E
134E
136E
138E
11
10
9
8
7
6
5
3 & 4
August
JMA_BT
EC_CE
EC_SEa

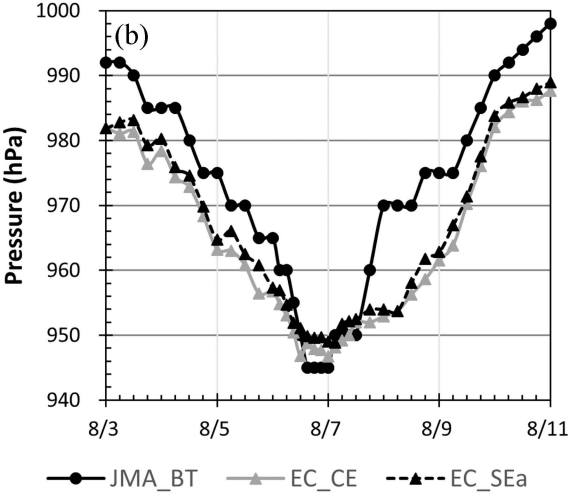
(b)
Pressure (hPa)
1000
990
980
970
960
950
940
8/3
8/5
8/7
8/9
8/11
JMA_BT
EC_CE
EC_SEa

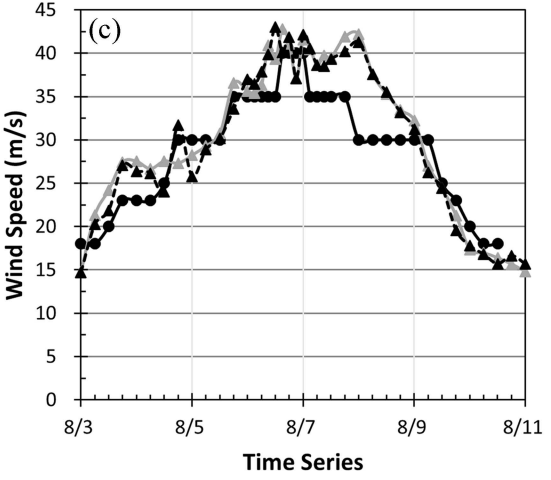
(c)
Wind Speed (m/s)
45
40
35
30
25
20
15
10
5
0
8/3
8/5
8/7
8/9
8/11
Time Series

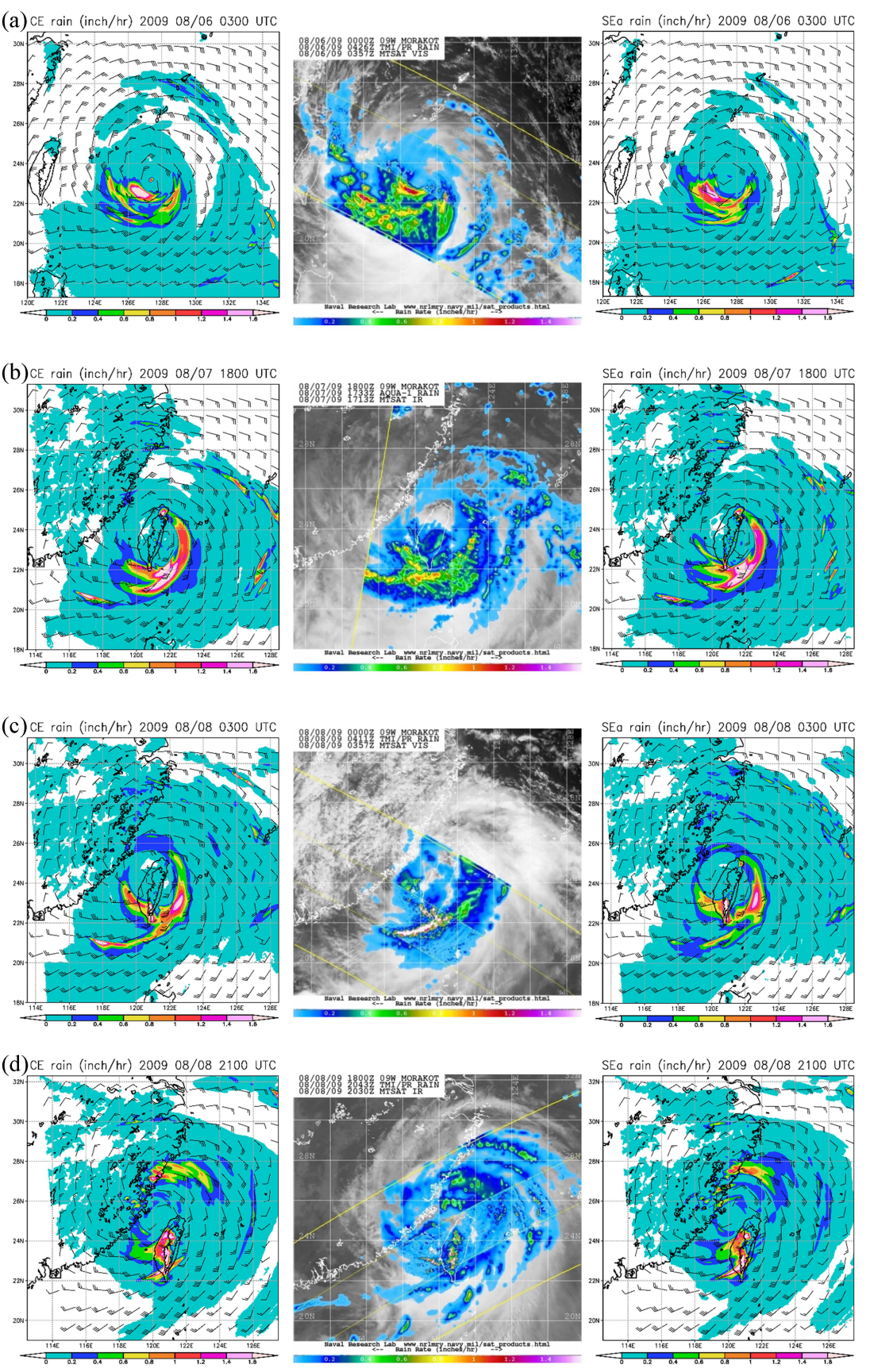
(a)
CE rain (inch/hr) 2009 08/06 0300 UTC
08/06/09 0000Z 09W MORAKOT
08/06/09 0426Z TMI/PR RAIN
08/06/09 0357Z MTSAT VIS
SEa rain (inch/hr) 2009 08/06 0300 UTC
(b)
CE rain (inch/hr) 2009 08/07 1800 UTC
08/07/09 1800Z 09W MORAKOT
08/07/09 1733Z AQUA-1 RAIN
08/07/09 1713Z MTSAT IR
SEa rain (inch/hr) 2009 08/07 1800 UTC
(c)
CE rain (inch/hr) 2009 08/08 0300 UTC
08/08/09 0000Z 09W MORAKOT
08/08/09 0411Z TMI/PR RAIN
08/08/09 0357Z MTSAT VIS
SEa rain (inch/hr) 2009 08/08 0300 UTC
(d)
CE rain (inch/hr) 2009 08/08 2100 UTC
08/08/09 1800Z 09W MORAKOT
08/08/09 2043Z TMI/PR RAIN
08/08/09 2030Z MTSAT IR
SEa rain (inch/hr) 2009 08/08 2100 UTC
Naval Research Lab www.nrlmry.navy.mil/sat_products.html
<-- Rain Rate (inches/hr) -->

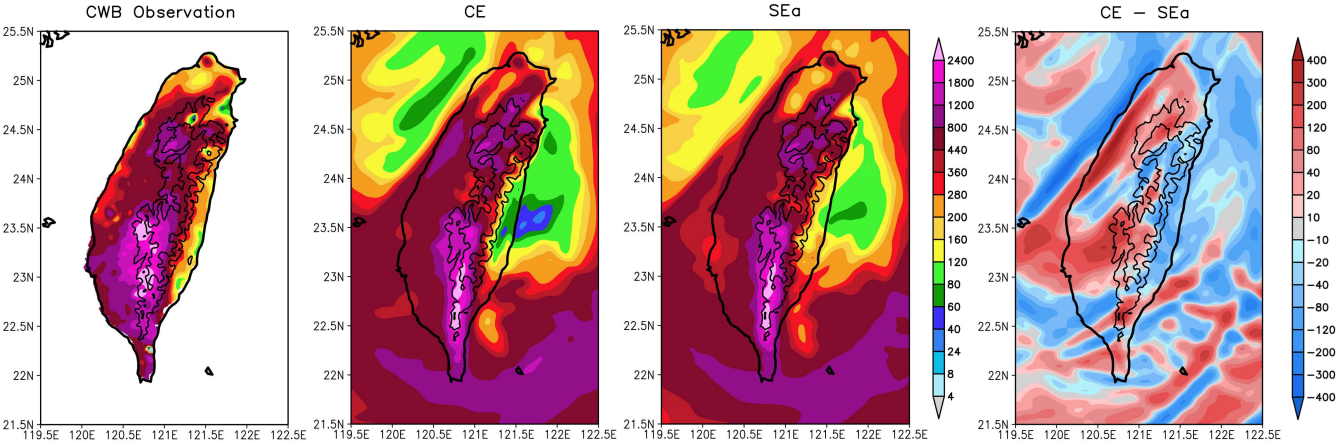
CWB Observation
CE
SEa
CE − SEa
25.5N
25N
24.5N
24N
23.5N
23N
22.5N
22N
21.5N
119.5E
120E
120.5E
121E
121.5E
122E
122.5E
2400
1800
1200
800
440
360
280
200
160
120
80
60
40
24
8
4
400
300
200
120
80
40
20
10
−10
−20
−40
−80
−120
−200
−300
−400

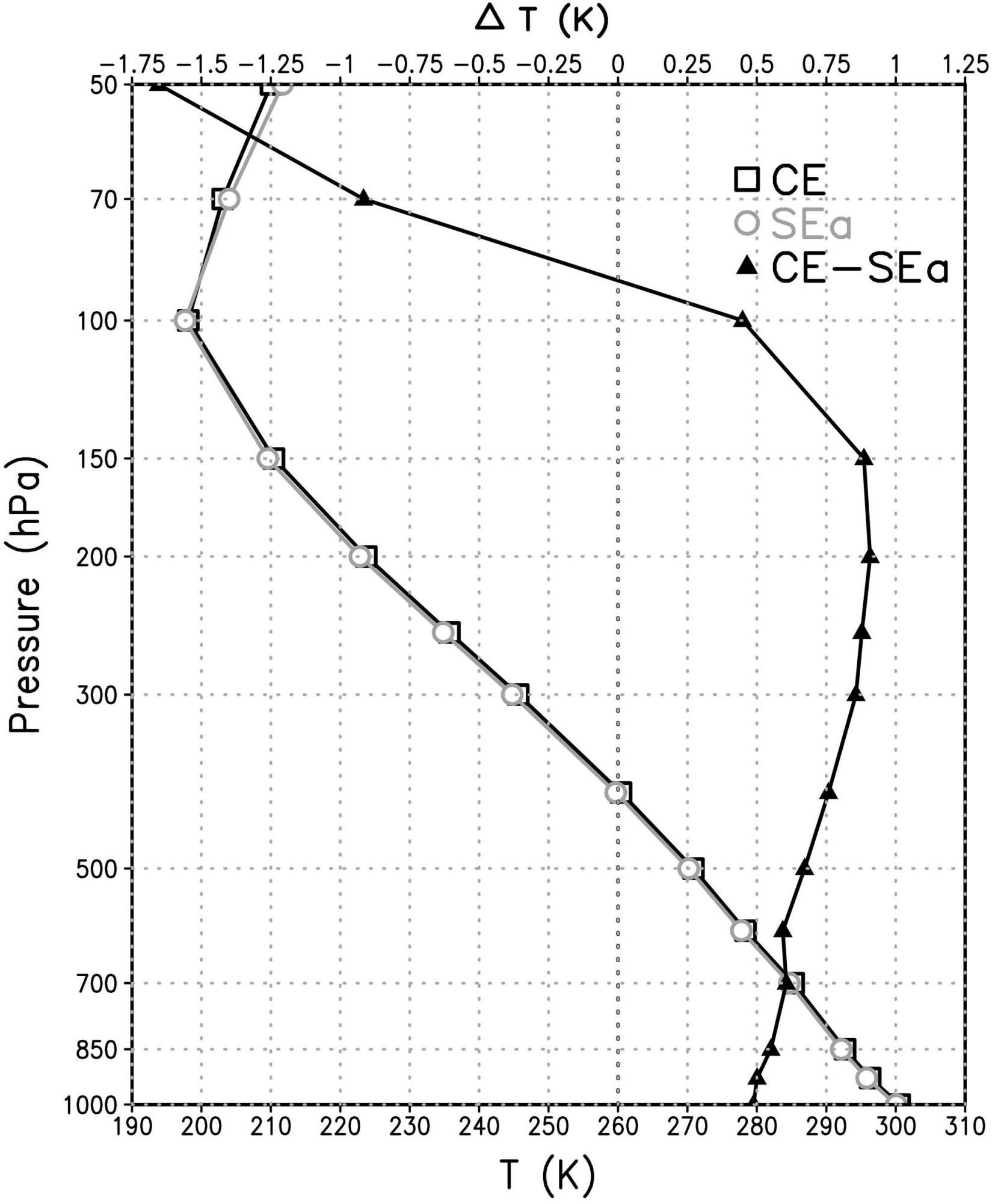
Δ T (K)
−1.75 −1.5 −1.25 −1 −0.75 −0.5 −0.25 0 0.25 0.5 0.75 1 1.25
50
70
100
150
200
300
500
700
850
1000
Pressure (hPa)
CE
SEa
CE−SEa
190 200 210 220 230 240 250 260 270 280 290 300 310
T (K)